Contribution to the Modeling and Simulation of the Iron-Based Chemical Looping Combustion Process

Ana-Maria Cormos* and Dora-Andreea Chisalita[a]

The increasing concentrations of greenhouse gases in the atmosphere are directly linked to climate change. Given that most of the world's electric energy comes from fossil-fuel power plants, which produce a large amount of greenhouse gas (i.e., CO_2), carbon capture and storage technologies seem to be a viable solution to reduce CO_2 emissions. To investigate fossil-fuel chemical looping combustion in fluidized bed columns, a dynamic mathematical model was herein developed. The complex phenomena taking place in the iron-based chemical looping combustion process are described by assuming a pseudo-homogeneous system and a plug–flow regime for the fluidized columns. The mass and energy balance equations were written by using partial differential equations for both the gaseous and solid phases present in the process. The distribution and temperatures profiles of the gaseous and solid components as well as a study on the influence of the superficial gas velocity on the particle distribution were generated by model simulation. This computational approach allows for significant progress in the systematic analysis of chemical looping combustion to assess its potential for integration into the next generation of fossil-fuel power plants.

Introduction

The greenhouse effect is a natural phenomenon occurring in the atmosphere of a planet caused by greenhouse gases. Increased concentrations of greenhouse gases, mainly CO_2, upset the natural balance of the greenhouse effect, which leads to an increase in the average mean temperature, a phenomenon known as global warming.

There are numerous methods for reducing greenhouse gases emission into the atmosphere, such as reducing the global energy consumption by increasing the efficiency of energy conversion/consumption or by turning to alternative energy sources (e.g., wind or solar energy).[1] However, as most of the world's electric energy comes from coal power plants, which produce a large amount of CO_2, carbon capture and storage (CCS) technologies seem to be a viable solution, because they have the potential to reduce CO_2 emissions by 90%.

There are several carbon-capture technologies that are already available that can be classified on the basis of the position of the carbon-capture unit in technological flow in post-combustion, precombustion, and oxycombustion. A very promising technology with inherent separation of CO_2 is chemical looping combustion (CLC) (Figure 1).[1,2]

From a general point of view, CLC is a technology based on the existence of a reactive solid material (i.e., oxygen carrier) that circulates between two interconnected fluidized bed reactors to drive the chemical reaction.

The oxygen carrier sustains a series of redox cycles and is oxidized in the air reactor (AR) and reduced in the fuel reactor (FR). In this way, there is no direct contact between air and the fuel, and the process can deliver a high-purity stream of CO_2. The oxidizing/reducing gas is introduced at the bottom of the columns and acts as a fluidizing agent for the solid material. The mixture of gases and solids leaves the fluidized reactors through a cyclone. The oxygen carries particles fall from the cyclone through vertical stand pipes to the bottom of the fluidized columns.

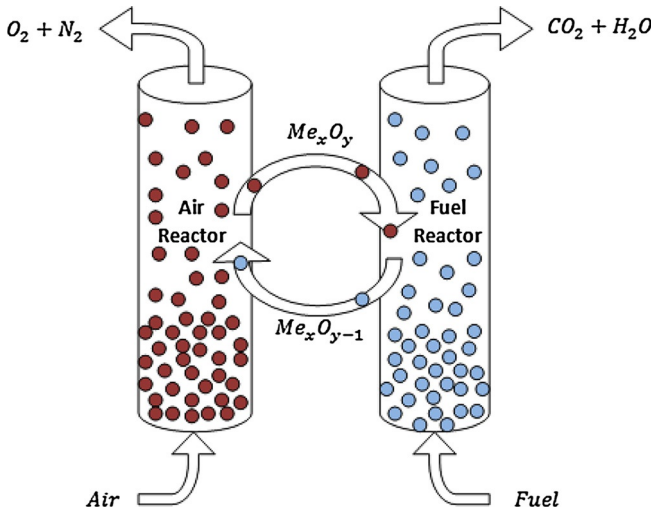

Figure 1. Chemical looping combustion layout.

The fuel in the combustion step of the chemical-looping process can be gaseous, liquid, or solid. Solid fuels represent

[a] Dr. A.-M. Cormos, D.-A. Chisalita
Chemical Engineering Department, Babes-Bolyai University
Arany Janos 11, RO-400028 Cluj-Napoca (Romania)
E-mail: cani@chem.ubbcluj.ro
The ORCID identification number(s) for the author(s) of this article can be found under http://dx.doi.org/10.1002/ente.201600030.

Part of a Special Issue on "Chemical Looping for Energy Technologies". To view the complete issue, visit:
http://dx.doi.org/10.1002/ente.v4.10/

the majority of fossil resources in the world, and as a consequence, the chemical looping combustion of solid fuels can be considered as a very attractive solution for carbon capture.

In comparison to solid fuels, liquid and gaseous fuels can be more easily converted in a chemical looping process. Gasification of the solid fuel, followed by cooling and purification of the obtained gases could be a feasible way to use solid fuels in chemical looping combustion. The composition of the synthesis gas could vary, depending on the type of fuel used in the gasification process. Syngas in general contains 20–40 % H_2, 35–40 % CO, 25–35 % CO_2, 0–15 % CH_4, and 2–5 % N_2.[3] The synthesis gas may also contain impurities such as solid particles, ammonia, and mercury; therefore, a particle removal unit must precede the sulfur removal stage. After these steps, syngas can be fed into the fuel reactor.[4,5] The oxygen carrier particles have to pass a cyclone separator before they can be transferred from one reactor to another. A simplified layout of the overall process of CLC including gasification of the solid fuel is presented in Figure 2.

The development of the chemical looping combustion process over the past 15 years has led to new information regarding a range of engineering challenges that need to be overcome to use the process commercially. The design and operation conditions of the reactor, thermodynamic and kinetic analysis, as well as the development of new and improved oxygen carrier materials have to be done before implementation of the process to industrial scale.

There are various testing facilities all over the world. At the Chalmers University of Technology, Sweden, a 10 kW facility was first used to perform various tests for solid fuels by using ilmenite as the oxygen carrier,[6–8] and later, a 100 kW chemical looping plant was built. A 25 kW unit was built both in Germany at the Hamburg University of Technology and in the USA at Ohio State University by using different reactor designs. The largest pilot plant for chemical looping combustion by using iron ore can be found at the Technische Universität Darmstadt in Germany, and it has a nominal power of 1 MW_{th}. The largest chemical looping combustion pilot plant is the Alstom-GE plant, which generates 3 MW_{th} power and uses limestone as the oxygen carrier. The operational results obtained by using ilmenite as the oxygen carrier and hard coal as the fuel were presented by Ströhe et al. in 2014,[9] and simulations of the 1 MW_{th} CLC process performance, in a steady-state operation regime, were presented by Abad et al.[10a,b]

Also, experiments with gaseous fuels by using iron- and nickel-based oxygen carriers were performed in a 120 kW fuel power dual circulating fluidized bed installation at the Vienna University of Technology in Austria.[11] A 150 kW CLC reactor system working with gaseous fuels and inexpensive oxygen carriers derived from industrial byproducts or natural minerals such as manganese ore was designed at the Norwegian University of Science and Technology.[12]

The reactions in the fuel and air reactors are expressed by reactions (1) and (2), respectively.[1] Assuming the fuel from the FR as C_nH_{2m}, the reduction of the oxygen carrier can be written as follows:

$$(2n+m)\,Me_xO_y + C_nH_{2m} \rightarrow (2n+m)\,Me_xO_{y-1} + n\,CO_2 + m\,H_2O \quad (1)$$

in which Me_xO_y is the metal oxide and Me_xO_{y-1} is its reduced counterpart. The exhaust gases leaving the fuel reactor contain only carbon dioxide and water, which can be easily removed by condensation, and this avoids the large costs and energy penalties of gas separation present in other CCS technologies. The solid flow leaving the FR is depleted in oxygen; the reduced oxygen carrier is carried back to the AR where it is regenerated following reaction (2).

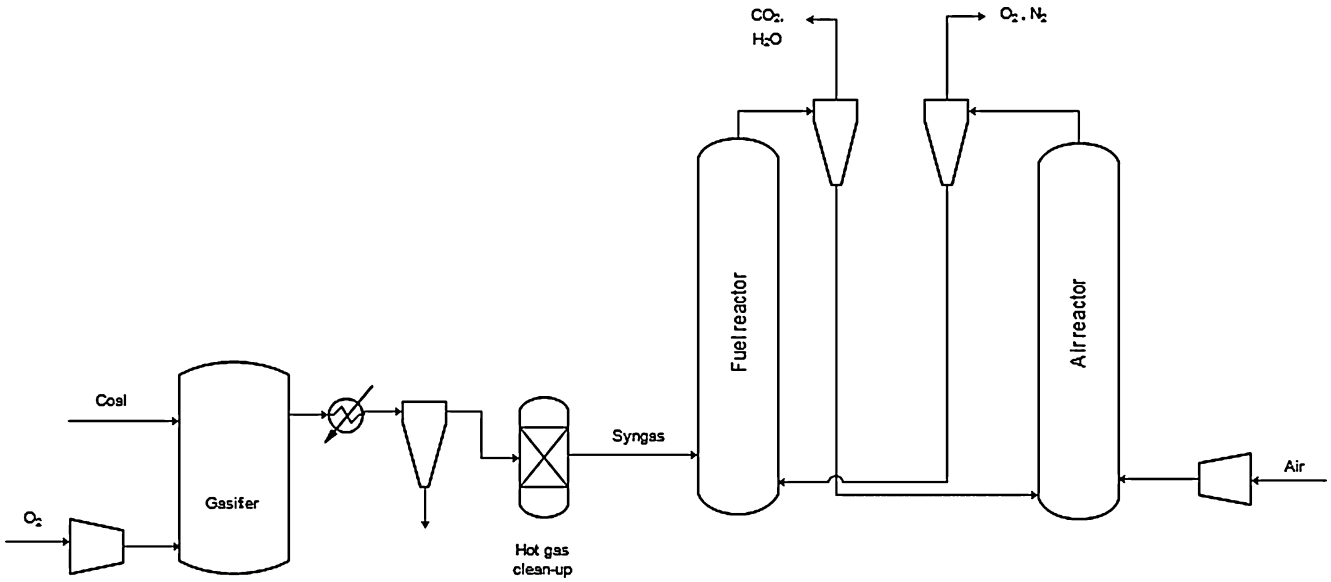

Figure 2. The syngas chemical looping combustion process with the major flows of the system.

$$Me_xO_{y-1} + {}^1/_2\,O_2 \rightarrow Me_xO_y \quad (2)$$

The majority of oxygen carriers proposed in the literature are synthetic materials based on transitional-metal oxides (e.g., CuO, NiO, Fe_2O_3, or Mn_3O_4) supported on inert materials (e.g., Al_2O_3, SiO_2, TiO_2, or ZrO_2). Nevertheless, owing to the much lower price of oxygen carriers based on natural ores or solid waste originating from industrial processes, these oxygen carriers were also taken into account as a promising alternative.[13]

Choosing the right oxygen carrier is important, as it should have certain properties such as high reactivity to fully convert the fuel into CO_2 and H_2O. The solid particles have to be mechanically resistant with a low attrition rate, because the particles are subjected to a number of fluidization cycles. Taking into account that the processes inside the reactors take place at high temperatures, the oxygen carrier should have a low agglomeration tendency and a high melting point. Furthermore, the carrier has to present low toxicity and be economically profitable.

Iron oxide has received significant attention for chemical looping combustion applications, as naturally occurring iron ores (such as magnetite, ilmenite, hematite, limonite, etc.) are inexpensive. The oxygen carrier used in this study is ilmenite, an iron and titanium ore ($FeTiO_3$). According to the literature, the reactivity of ilmenite increases after 5–20 redox cycles, also called the activation period, after which the reactivity remains mostly constant. The number of activation cycles relies upon the reduction rate reached in every cycle and the reducing gas used.[14] The activation process is relatively fast; therefore, it can be done inside the process.

Process modeling and simulation is a vital tool in the development of novel technology. To develop suitable control strategies that can be implemented in this process for on-line control, a dynamic process model is required. In the current work, a dynamic model was developed for the iron-based chemical looping combustion process for using natural gas and coal-derived syngas as fuels. The fuel reactor temperature is a key parameter that can be used to improve the performance of the process, and the developed model includes the energy balance equations coupled with mass balance.

The effect of the gas superficial velocity on the particle distribution in the fluidized bed and the efficiency of the process were investigated. To assess the effect of operational conditions on the performance of the CLC plant, the transient behavior of the air and fuel reactors was simulated through step changes in the input gas flow rate.

Model Development

Kinetics

The final product obtained during ilmenite oxidation with air depends on the reaction time and temperature. From Rao and Riguard's[15] experiments, three oxidation products were observed at different temperatures. Thus, hematite (Fe_2O_3) and titanium dioxide (TiO_2) were obtained between 773 and 1023 K, hematite and pseudorutile ($Fe_2Ti_3O_9$) were obtained between 1043 and 1163 K, and pseudobrookite (Fe_2TiO_5) and rutile (TiO_2) were identified as oxidation products at temperature above 1173 K. Donskoi[16] in the integrated rate of reaction (IRoR) model considered pseudobrookite as $Fe_2O_3 + FeO$, ilmenite as $FeO + TiO_2$, magnetite as $Fe_2O_3 + FeO$, and titanium dioxide as an inert material. Therefore, Abad et al.,[17] proposed, on the basis of experimental data, that the oxidation and reduction reactions of activated ilmenite could be expressed in a simplified manner as presented in reactions (3)–(6), for which Fe_2O_3 represents all the ferric compounds and FeO represents all the ferrous ones.[17] Gaseous components from coal-derived syngas were used as the reducing agents.

$$4\,FeO + O_2 \rightarrow 2\,Fe_2O_3 \quad (3)$$

$$Fe_2O_3 + CO \rightarrow 2\,FeO + CO_2 \quad (4)$$

$$Fe_2O_3 + H_2 \rightarrow 2\,Fe + H_2O \quad (5)$$

$$4\,Fe_2O_3 + CH4 \rightarrow 8\,FeO + CO_2 + 2\,H_2O \quad (6)$$

To describe the kinetics of the process, a mixed model was used, as proposed by Abad,[17] that combines the grain model with a uniform reaction in the particle and changing grain size model in the grains. The model assumes that the oxygen carrier particle consists of a number of spherical, nonporous grains with equal initial radius.[18] The reaction takes place in the grain following the shrinking core model (see Figure 3).

Assuming that the reaction rate of the process is controlled by the chemical reaction taking place in the grain, mass transfer of the gas film and diffusion inside the particle can be neglected, so the equations that describe this reaction

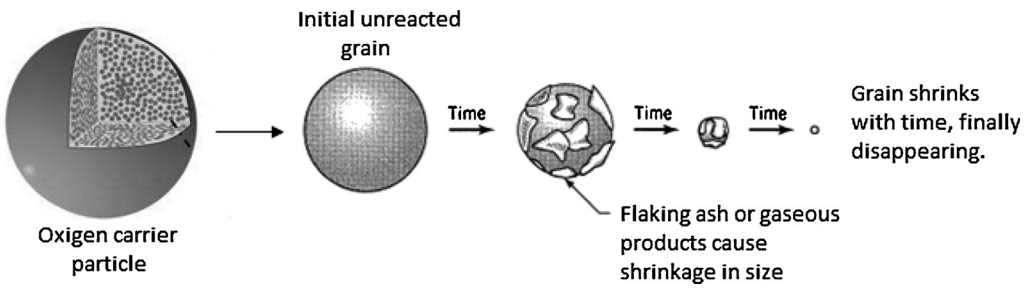

Figure 3. Detailed view of the grain model.[19]

model are the following [Eqs. (7)–(9); the symbol definitions are presented in a separate section at the end of the manuscript]:

$$\frac{dX_{OC}}{dt} = \left[\frac{3}{\tau}\cdot(1-X_{OC})^{\frac{2}{3}}\right] \quad (7)$$

$$\tau = \frac{\rho_m \cdot r_g}{b \cdot k_s \cdot C_g^n} \quad (8)$$

$$k_S = k_{S0}\cdot e^{-E_a/RT} \quad (9)$$

The kinetic parameters for this model in the case of ilmenite reduction and oxidation are presented in Table 1.[17]

The influence of gas compositions on the performance of the oxidation and reduction processes, according to the experimental results and kinetics model published by Abad et al.,[17] is presented in Figure 4a,b. As previously shown,[17] in the case of the oxidizing gas, upon increasing the oxygen composition the maximum conversion is reached in a shorter amount of time. The same results are obtained for the reduction step.

Balance equations

The complex heterogeneous phenomena that take place in the CLC process are described with consideration of the following assumptions:[18]

1) Perfectly spherical solid particles with a constant diameter and permanent macroscopic structure
2) Pseudo-homogeneous system within the elementary segment dz in both reactors
3) Plug–flow regime for both reactors
4) 1D hydrodynamic model developed by Kunii and Levenspiel[20]

The mass and energy balance equations were written by using partial differential equations for both the gaseous and solid phases present in the process.[18,21] For the fluidized bed reactors system, the balance equations are shown in Equations (10) and (11) and in Equations (13) and (14).

Total mass balance:

$$\frac{1}{w_j}\cdot\frac{\partial F_j}{\partial t} = -\frac{\partial F_j}{\partial z} \pm S\cdot\frac{\alpha\cdot M_i}{\beta\cdot M_{FeO/Fe_2O_3}} \quad (10)$$

Component mass balance:

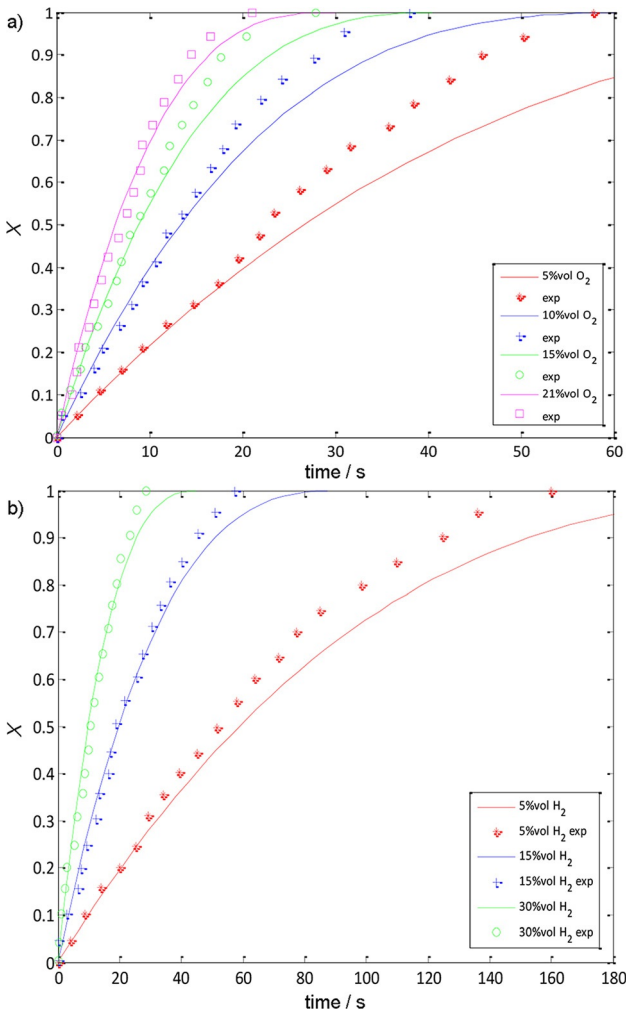

Figure 4. The influence of the gas concentration on the conversion process of ilmenite: a) oxidation process and b) reduction process.[17]

$$\frac{1}{w_j}\cdot\frac{\partial(F_j\cdot x_i)}{\partial t} = -\frac{\partial(F_j\cdot x_i)}{\partial z}\sum S_i\cdot\frac{\alpha\cdot M_i}{\beta\cdot M_{FeO/Fe_2O_3}} \quad (11)$$

in which F_j refers to the mass flow of both the gaseous and solid phases present in the reactors, w_j is the flow rate of each phase, α and β are stoichiometric coefficients (α is the stoichiometric coefficient of component i and β is the stoichiometric coefficient of the solid component from the heterogeneous gas–solid reactions), and M_i is the molecular weight of component i. The $\pm$ sign indicates the direction of the mass transfer represented by the heterogeneous reaction source term, S described in Equation (12). M_{FeO/Fe_2O_3} is the

Table 1. Kinetic parameters of activated ilmenite particles.[17]

Reaction	Molar density ρ_m[mol m^{-3}]	Grain radius r_g [m]	Average stoichiometric coefficient, b	Pre-exponential factor k_{s0} [mol m s^{-1}]	Activation energy E_a [kJ mol^{-1}]	Reaction order n
oxidation with O_2	31 100	1.2×10^{-6}	4	1.9×10^{-3}	25.5 ± 1.2	1
reduction with CH_4	13 590	1.25×10^{-6}	5.78	9.8	135.2 ± 6.6	1
reduction with H_2	13 590	1.25×10^{-6}	1.45	6.2×10^{-2}	65 ± 2.7	1
reduction with CO	13 590	1.25×10^{-6}	1.45	0.1	80.7 ± 2.4	0.8

molecular weight of FeO for the oxidation reaction, and, respectively, Fe_2O_3 for the reduction reaction.

$$S = \frac{v_p \cdot F_{oc}}{w_s} \tag{12}$$

In the component mass balance, x_i is the mass fraction of the components, which are FeO and Fe_2O_3 for the solid phase, O_2 and N_2 for the gaseous phase present in the air reactor, and H_2, CO, CH_4, CO_2, and H_2O for the gaseous phase present in the fuel reactor.

The energy balance equations [Eqs. (13) and (14)] were written knowing that the oxidation reaction is exothermic, whereas the reduction reaction is endothermic.

Energy balance (gas and solid phase):

$$\frac{1}{w_g} \cdot \frac{\partial(F_g \cdot Cp_g \cdot T_g)}{\partial t} = -\frac{\partial(F_g \cdot Cp_g \cdot T_g)}{\partial z} - H_{gs} - H_{gw} \tag{13}$$

$$\frac{1}{w_s} \cdot \frac{\partial(F_s \cdot Cp_s \cdot T_s)}{\partial t} = -\frac{\partial(F_s \cdot Cp_s \cdot T_s)}{\partial z} - H_{gs} - H_{sw} - H_r \tag{14}$$

In multiphase systems, the heat transfer characteristics are strongly influenced by the properties of the particle, such as size, size distribution, and shape, but they are also influenced by the operating conditions of the fluidized bed, which leads to different bed structures and, therefore, to varied heat transfer coefficients. With respect to gas–solid heat transfer, the theoretical and experimental models that describe this phenomenon are not as numerous as those regarding heat/energy transfer between the fluidized bed and the reactor's wall. Despite the large variety of models, it is still very difficult to estimate the heat transfer coefficients, because different researchers have reported distinct values for the same experimental conditions. However, as a result of these studies, the following conclusions were drawn:[22,23]

1) Inside the fluidized bed, the temperature of the gas is constant, except for a boundary layer close to the reactor's walls, at which a large temperature gradient appears. For this reason, the global heat transfer coefficient between the bed and the wall is greater than in the case of a monophasic system
2) The gas–solid contact area becomes much greater as the diameter of the grains decreases, especially in the case of micrograins
3) As the movement of the solid particle in the fluidized bed becomes faster, heat transfer between the phases is intensified, which maintains the temperature in the fluidized column to an almost constant value.

The heat fluxes involved in the energy balance are described in Equations (15)–(18):

Heat transfer from gas to solid:

$$H_{gs} = K_{T_{gs}} \cdot A_{T_{gs}} \cdot (T_g - T_s) \tag{15}$$

Heat transfer from gas to wall:

$$H_{gw} = K_{T_{gw}} \cdot A_{T_{gw}} \cdot (T_g - T_w) \tag{16}$$

Heat transfer from solid to wall:

$$H_{sw} = K_{T_{sw}} \cdot A_{T_{sw}} \cdot (T_s - T_w) \tag{17}$$

Heat of reaction:

$$H_r = \Delta H_r \cdot S \cdot \frac{1}{M_{FeO/Fe_2O_3}} \tag{18}$$

Hydrodynamics

To describe the hydrodynamics of the heterogeneous process, the 1D model developed by Kunii and Levenspiel was used.[20] The 1D model shows that the particle distribution in the fluidized bed reactor is based on the type of solid inventory present in the reactor and the superficial gas velocity. According to the model, the fluidized bed will be divided into two zones: a dense zone at the bottom of the bed that has a constant solid fraction and a lean zone at the upper part of the reactor, above the dense zone, in which the solid fraction decreases with height.

To have a fluidized bed, the fluidizing gas velocity has to exceed the minimum fluidization velocity, u_{mf}. A widely used correlation for determining the minimum fluidization velocity is Equation (19):[23]

$$Re_{umf} = \frac{d_p \cdot u_{mf} \cdot \rho_g}{\mu} = \sqrt{K_1{}^2 + K_2 \cdot Ar} - K_1 \tag{19}$$

in which $K_1 = 27.2$ and $K_2 = 0.0408$[10a,24] and the Archimedes number has the following expression [Eq. (20)]:

$$Ar = \frac{d_p^3 \cdot \rho_g \cdot (\rho_s - \rho_g) \cdot g}{\mu^2} \tag{20}$$

For the solid particles to follow the fluidizing gas and eventually leave the reactor, the fluidizing gas velocity has to exceed the terminal velocity, u_t, which can be expressed through a dimensionless particle diameter, $d_p{}^*$, and a dimensionless velocity, $u_t{}^*$, which resolves Equations (21) and (22) into (23).[20]

$$d_p^* = d_p \cdot \left[\frac{\rho_g \cdot (\rho_s - \rho_g) \cdot g}{\mu^2}\right]^{\frac{1}{3}} \tag{21}$$

$$u_t^* = \left[\frac{18}{\left(d_p^*\right)^2} + \frac{0.591}{\left(d_p^*\right)^{0.5}}\right]^{-1} \quad (22)$$

$$u_t = u_t^* \cdot \left[\frac{\mu \cdot (\rho_s - \rho_g) \cdot g}{\rho_g^2}\right]^{1/3} \quad (23)$$

The height of the dense zone, H_d, can be calculated as the difference between the total height of the reactor, H_t, which is known, and the height of the lean zone, H_l, which has the following expression [Eq. (24)]:

$$H_l = \frac{1}{a}\ln\left(\frac{\varepsilon_{sd} - \varepsilon_s^*}{\varepsilon_{se} - \varepsilon_s^*}\right) \quad (24)$$

in which a is the decay constant for the solid fraction in the lean zone, and according to Geldart's classification of particles it has different values. In the present case, the particles used in this study can be classified as Geldart B solids, so $au_0 = 7\,s^{-1}$. The volume fraction of solids in the dense region, ε_{sd}, has values between 0.4 and 0.22 for a turbulent bed. In this study, a value of 0.3 was assumed. To determine the carrying capacity of the gas, ε_s*, and the volume fraction of solids at the reactor exit, ε_{se}, a saturated flux of solids out of the reactor, G_{sat}*, has to be calculated [Eqs. (25)–(27)]:

$$G_{sat}^* = 23.7 \cdot \rho_g \cdot u_0 \cdot \exp\left(-5.4 \cdot \frac{u_t}{u_0}\right) \quad (25)$$

$$\varepsilon_s^* = \frac{G_{sat}^*}{u_0 \cdot \rho_s} \quad (26)$$

$$\varepsilon_{se} = \frac{G_{sat}^*}{(u_0 - u_t) \cdot \rho_s} \quad (27)$$

Results and Discussion

The mass and energy balance equations together with the equations that describe the hydrodynamics of the process were implemented in MATLAB/Simulink by using the design and operational parameter of the 1 MW_{th} pilot plant from Darmstadt University (see Table 2).[9,10a,25]

The simulation results were compared to data published in the literature by Abad[10a] to validate the mathematical model. The mass fractions of the inlet and outlet gases obtained by simulation as well as experimental data (published in the literature) are presented in Table 3. The results of the chemical looping combustion cycle for this simulation are in line with the literature data. The flow, composition, and temperature profiles of both the solid and gaseous phases present in the chemical looping combustion process as well as a study on the influence of the superficial gas velocity on the particle distribution were generated by simulation. Two study cases were investigated by using natural gas and coal-derived syngas as fuel.

Table 3. Validation data.

Gaseous component	Inlet [wt%]	Literature outlet[10a] [wt%]	Simulated outlet [wt%]
H_2	2.22	0.3	0.7
CO	10.12	4.1	4.08
CH_4	3.12	0.07	1.2
CO_2	24.47	39.76	30.82
H_2O	60.07	55.77	63.2

From Figure 5 we can notice that FeO is consumed almost entirely in the dense zone of the air reactor, and more than 80% of the oxidation reaction takes place in this area. The discontinuity in the flow profiles is line with the particle distribution, with the end of the dense zone and the beginning of the lean zone. Similar profiles can be seen for the gas composition in the natural gas fuel reactor in Figures 6 and 7.

Oxidized solid oxygen carrier flow and solid temperature profiles in both fluidized reactors are presented in Figure 8. As can be observed, the outlet flow of the air reactor is the inlet of the fuel reactor. The solid-phase temperature in the lower part of the dense zone of the air reactor increases as a result of the exothermic reaction that takes place in the

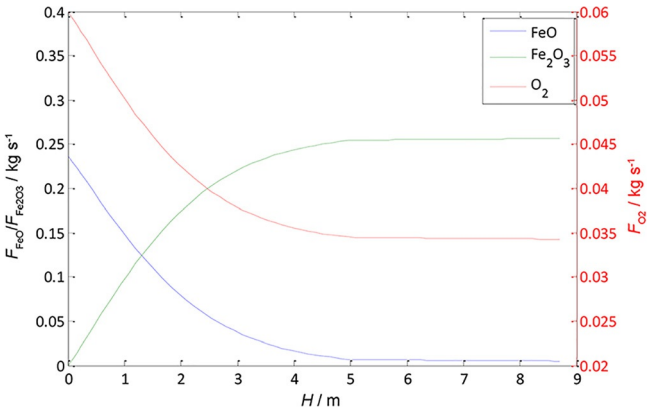

Figure 5. Air reactor flow profiles.

Table 2. Design and operation parameters.[9,10a,25]

Reactor	Height H [m]	Diameter D [m]	Temperature T [K]	Superficial gas velocity, u_0 [m s^{-1}]	Solid circulation rate, F_{oc} [kg s^{-1}]	Particle diameter d_p [μm]
air reactor	8.7	0.59	1323	3.5	0.55–2.5	250
fuel reactor	11.4	0.4	1273	3.5	0.55–2.5	250

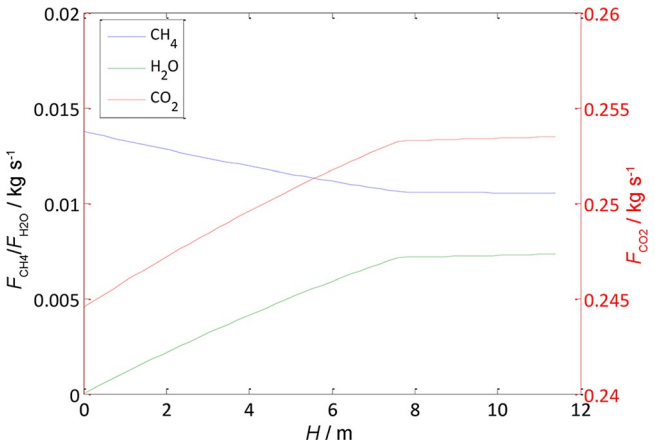

Figure 6. Gas composition profiles for natural-gas fuel reactor.

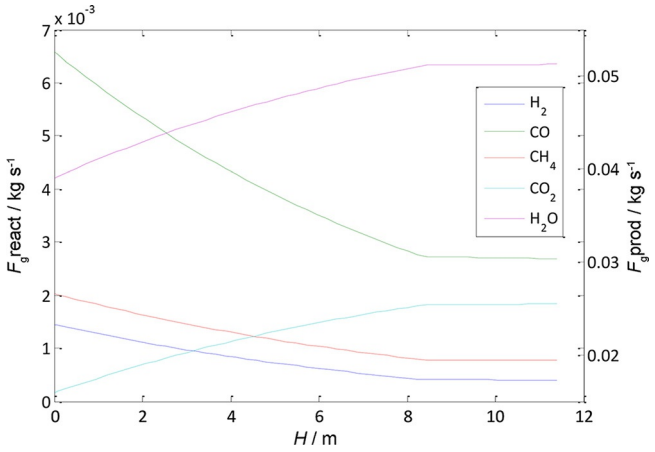

Figure 7. Gas flow profiles for syngas fuel reactor.

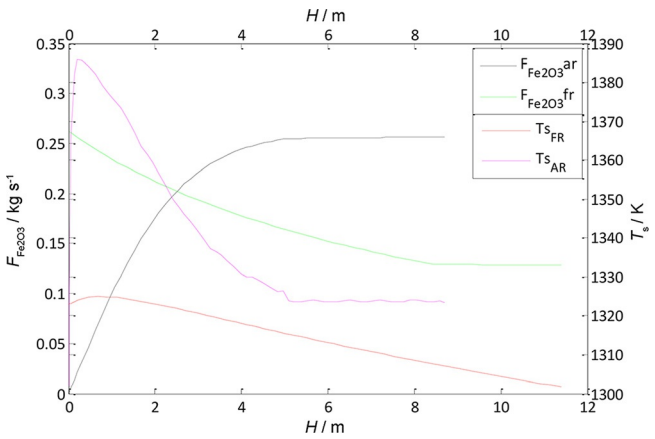

Figure 8. The oxygen carrier flow and solid temperature profiles in both fluidized reactors.

grain, after which the temperature drops and reaches a constant value equal to the inlet temperature of the fuel reactor.

In the FR, because of the endothermic reaction that takes place, the temperature of the solid phase decreases until a certain temperature (the inlet temperature of the air reactor).

The particle distribution in the fluidized bed is influenced by the gas superficial velocity. The height of the dense region decreases upon increasing the superficial velocity of the gas (Figure 9). To achieve a higher oxidation/ reduction of the

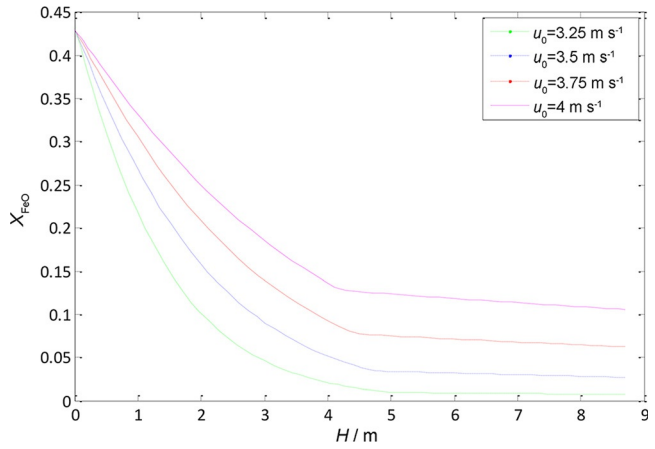

Figure 9. Solid (FeO) distribution in the syngas fuel reactor with variable superficial gas velocity.

oxygen carrier, a smaller gas superficial velocity has to be used. A change in the gas velocity from 3.25 to 4 $m s^{-1}$ for the syngas fuel reactor results in a decrease in the height of the dense region from 5.10 to 4.20 m. The oxidation reaction efficiency significantly decreases from 96 to 59%. In the case of the natural gas fuel reactor (Figure 10), changing the gas velocity from 3 to 3.5 $m s^{-1}$ results in a decrease in the height of the dense zone from 8.20 to 7.63 m, and the output concentration of the natural gas increases significantly from 0.03 to 0.038 wt%

To study the effect of the operation conditions on the chemical looping combustion process, the transient behavior of the air and fuel reactors was simulated by increasing the input gas flow rate by 20% (Figures 11 and 12). The simulation results show that the efficiency of the reduction and oxi-

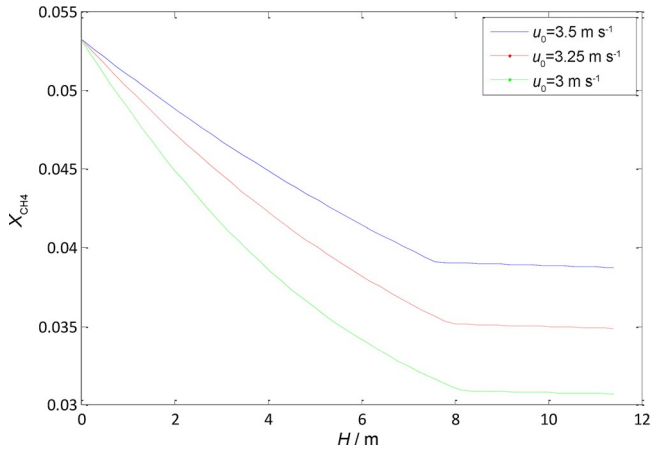

Figure 10. The CH_4 concentration profiles in the natural gas fuel reactor with variable superficial gas velocity.

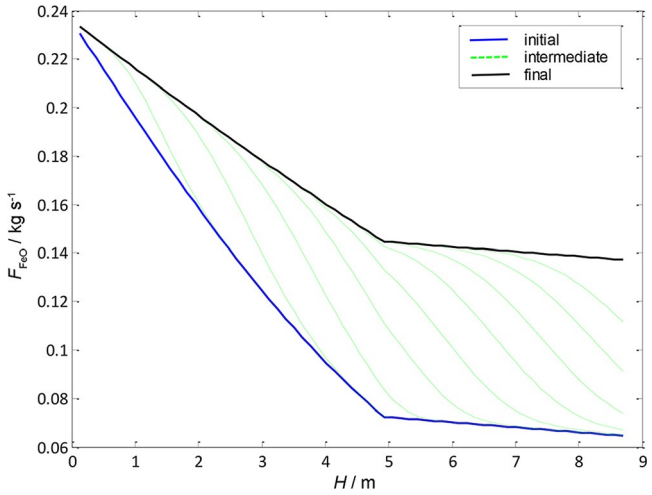

Figure 11. FeO flow variation with a 20% increase in the inlet gas flow in the AR.

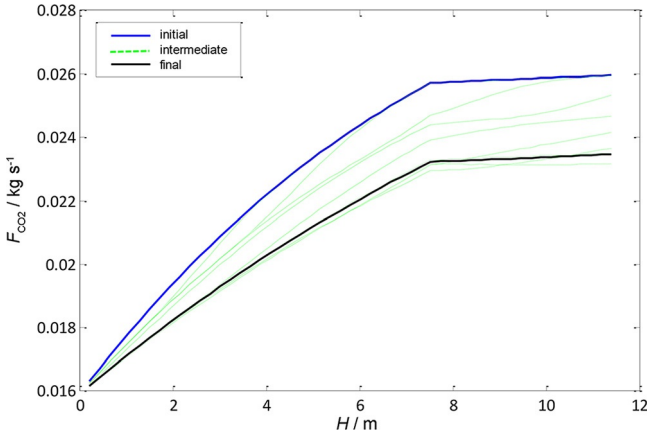

Figure 12. CO_2 flow variation with a 20% increase in the inlet flow in the FR.

dation reactions of the oxygen carrier significantly decreases upon increasing the gas flow rate.

Conclusions

In this study, a dynamic mathematical model for the iron-based chemical looping combustion process was developed. Two study cases, natural gas and coal-derived syngas as fuel, were investigated. The flow and temperature profiles, distributions of gaseous and solid components, and conversions of reactants were generated by simulation.

The simulation results showed that the oxidation and reduction reactions take place predominantly in the dense region of the fluidized bed reactor, because of the high, relatively constant solid concentration in this area.

The superficial gas velocity was shown to have a significant influence over the performance of the process; increasing the superficial gas velocity led to faster fluidization, for which more particles were carried out of the fluidized bed; this resulted in a decrease in the height of the dense zone and implicitly led to a lower conversion rate.

The dynamic behavior of the chemical looping combustion process resulting from step changes in the load flue gas was investigated. The efficiency with which the oxygen carrier performed the reduction/oxidation reactions significantly decreased upon increasing the gas flow rate.

The results obtained by simulation can be used to evaluate different operating conditions and to optimize and design an advanced control scheme of the chemical looping combustion process.

Nomenclature

Symbols

a	decay constant for the solid fraction in the lean zone
A_T	heat transfer area [$m^2\,m^{-1}$]
$\bar{b}$	average stoichiometric coefficient for gas–solid reactions
C_g	concentration of the reducing/oxidizing gas [$mol\,m^{-3}$]
C_p	specific heat capacity [$j\,mol^{-1}\,K^{-1}$]
d_p	diameter of the particle [m]
E_a	activation energy [$j\,mol^{-1}$]
F_j	mass flow of gaseous/solid phases present in the reactors [$kg\,s^{-1}$]
F_{oc}	circulation rate of the oxygen carrier [$kg\,s^{-1}$]
g	gravitational acceleration [$m\,s^{-2}$]
G_{sat}	saturated flux of solids out of the reactor
H	heat transfer flux [$J\,s^{-1}$]
H_l	height of lean zone [m]
H_d	height of dense zone [m]
k_S	kinetic constant [s^{-1}]
k_{S0}	pre-exponential factor [$mol\,m\,s^{-1}$]
K_T	heat transfer coefficient [$J\,m^{-2}\,s^{-1}\,K^{-1}$]
M	molecular weight of component i [$g\,mol^{-1}$]
n	reaction order
R	ideal gas constant [$J\,mol^{-1}\,K^{-1}$]
r_g	radius of grain [m]
S	heterogeneous reaction source term [$kg\,s^{-1}\,m^{-1}$]
t	simulation time [s]
T	temperature [K]
u_0	velocity of the superficial inlet gas [$m\,s^{-1}$]
u_{mf}	minimum fluidization velocity [$m\,s^{-1}$]
u_t	terminal velocity [$m\,s^{-1}$]
v_p	reaction rate [s^{-1}]
w_j	flow rate of solid/gaseous phase [$m\,s^{-1}$]
x_i	mass fraction of component i
X_{OC}	conversion of the oxygen carrier

Greek letters

α	stoichiometric coefficient of component i
β	stoichiometric coefficient of the solid component in the heterogeneous reaction
ΔH_r	heat of reaction [$J\,mol^{-1}$]
ε_{sd}	volume fraction of solids in the dense region

ε_{se} volume fraction of solids at the reactor exit
ε_s carrying capacity of the gas
μ dynamic viscosity [Pa s]
ρ_i mass density of solid/gaseous phase [kg m^{-3}]
ρ_m molar density of the solid particles [mol m^{-3}]
τ time for complete conversion of solid [s]

Subscripts/superscripts

g gas
s solid
w wall
i component
j phase
r reaction
* dimensionless

Acknowledgements

This work was supported by the Romanian National Authority for Scientific Research UEFISCDI, grant number ID-PCE-2011-3-0028: "Innovative methods for chemical looping carbon dioxide capture applied to energy conversion processes for decarbonized energy vectors poly-generation".

Keywords: carbon storage · chemical looping combustion · gas velocity · iron · mathematical modeling

[1] J. Adanez, A. Abad, F. Garcia-Laabiano, P. Gayan, L. F. de Diego, *Prog. Energy Combust. Sci.* **2012**, *38*, 215–282.
[2] Q. Imtiaz, D. Hosseini, C. R. Muller, *Energy Technol.* **2013**, *1*, 633–647.
[3] C. C. Cormos, A. M. Cormos, L. Petrescu, *Chem. Eng. Res. Des.* **2014**, *92*, 741–751.
[4] F. Li, H. R. Kim, D. Sridhar, F. Weng, L. Zeng, J. Chen, L.-S. Fan, *Energy Fuels* **2009**, *23*, 4182–4189.
[5] A. Tong, S. Bayham, M. V. Kathe, L. Zeng, S. Luo, L.-S. Fan, *Appl. Energy* **2014**, *113*, 1836–1845.
[6] N. Berguerand, A. Lyngfelt, *Energy Procedia* **2009**, *1*, 407–414.
[7] N. Berguerand, A. Lyngfelt, *Fuel* **2010**, *89*, 1749–1762.
[8] C. Linderholm, A. Cuadrat, A. Lyngfelt, *Energy Procedia* **2011**, *4*, 385–392.
[9] J. Ströhle, M. Orth, B. Epple, *Appl. Energy* **2014**, *113*, 1490–1495.
[10] a) A. Abad, P. Gayan, L. F. de Diego, F. Garcia-Labiano, J. Adanez, *Chem. Eng. Sci.* **2013**, *87*, 277–293; b) F. Garcia-Labiano, L. F. de Diego, P. Gayan, A. Abad, J. Adanez, *Chem. Eng. Sci.* **2013**, *87*, 173–182.
[11] T. Pröll, K. Mayer, J. Bolhàr-Nordenkampf, P. Kolbitsch, T. Mattisson, A. Lyngfelt, H. Hofbauer, *Energy Procedia* **2009**, *1*, 27–34.
[12] A. Bischi, Ø. Langørgen, I. Saanum, J. Bakken, M. Seljeskog, M. Bysveen, J.-X. Morin, O. Bolland, *Int. J. Greenhouse Gas Control* **2011**, *5*, 467–474.
[13] N. Berguerand, *Design and Operation of a 10 kW$_{th}$ Chemical-Looping Combustor for Solid Fuels*, PhD Thesis, Chalmers University of Technology, Gothenburg, Sweden, **2009**.
[14] J. Adánez, A. Cuadrat, A. Abad, P. Gayán, L. F. de Diego, F. Garcia-Labiano, *Energy Fuels* **2010**, *24*, 1402–1413.
[15] D. B. Rao, M. Rigaud, *Oxid. Met.* **1975**, *9*, 99–116.
[16] E. Donskoi, D. L. S. McElwain, L. J. Wibberley, *Metall. Mater. Trans. B* **2003**, *34*, 255–266.
[17] A. Abad, J. Adanez, A. Cuadrat, F. Garcia-Laabiano, P. Gayan, L. F. de Diego, *Chem. Eng. Sci.* **2011**, *66*, 689–702.
[18] A A. M. Cormos, D. A. Chisalita *Comput. Aided. Process. Eng.* **2016**, *38*, 271–276.
[19] O. Levenspiel, *Chemical Reaction Engineering*, 3rd ed., Wiley-VCH, Weinheim, **1999**, Chapter 25.
[20] D. Kunii, O. Levenspiel, *Chem. Eng. Sci.* **1997**, *52*, 2471–2482.
[21] A. M. Cormos, A. Simon, *Appl. Therm. Eng.* **2015**, *80*, 319–327.
[22] C. Mihaila, *Thermodynamic Processes in Gas–Solid Systems and Their Applications in Industry* (in Romanian), Technical Publisher, Bucharest, **1982**, Chapter 4.
[23] O. Levenspiel, D. Kunii, *Fluidization Engineering*, 2nd ed., Buteerworth-Heinemann, Stoneham, MA, **1991**, Chapters 3, 7.
[24] J. R. Grace, *Can. J. Chem. Eng.* **1986**, *64*, 353–363.
[25] A. Gunnarsson, *Process Simulation of a 1 MW$_{th}$ Chemical Looping Pilot Plant with Coal and Biomass as Fuel*, MSc Thesis, Chalmers University of Technology, Gothenburg, Sweden, **2014**.

Received: January 15, 2016
Published online on June 29, 2016

